







A Novel Miniaturized Strong-Coupled FSS Structure With Excellent Angular Stability

Tianwu Li , Da Li , Pengfei Qin , Yudi Fan, Yijie Gu, Panpan Zuo , *Member, IEEE*,
Wei E. I. Sha , *Senior Member, IEEE*, and Erping Li , *Fellow, IEEE*

Abstract—In this article, a novel miniaturized concept named strong-coupled frequency selective surface (SC-FSS) with excellent angular stability is presented. First, a conceptual design of SC-FSS is introduced, where the resonant frequencies are insensitive to almost all incident angles. A corresponding equivalent circuit model is developed to interpret the operating principle and formulate relevant design equations with an error of 0.2%. Furthermore, an ultraminiaturized and ultrathin band-stop structure with a unit cell size of $\lambda_0/35$ and thickness of 0.26 mm ($\lambda_0/578$) is designed and fabricated to verify this concept. Analysis and experiment show that the proposed band-stop SC-FSS structure can work stably at 2 GHz for both TE and TM modes, even when the incident angle varies from 0° to 84°. The measurement results are consistent with those obtained by full-wave simulations and the equivalent circuit model, which fully demonstrates that the concept of SC-FSS can be widely used in designing antenna reflectors, electromagnetic interference shielding, and angle-insensitive absorbers.

Index Terms—All-angle-insensitive, angular stability, equivalent circuit model (ECM), miniaturization, strong-coupled frequency selective surface (SC-FSS).

I. INTRODUCTION

FREQUENCY selective surface (FSS), a kind of spatial filters [1]–[5], has been widely used to design high-performance radome, antenna reflector, space electromagnetic interference (EMI) shielding, and electromagnetic stealth [6]–[10]. The multiband, wideband FSS, and the sharp band-edge structure have been investigated over the past years [11]–[16]. However, the resonant frequency of the FSS structure shifts under oblique incidence, which arises the angular instability

problem restricting the reliable engineering applications of FSS. In view of the angle-sensitive problem, a lot of research on the miniaturized FSS has been carried out [17]–[26]. First, Azemi *et al.* [20] and Ghosh and Srivastava [21] used meandered structures to increase the effective electrical length of patches, resulting in a larger equivalent inductance. However, due to the limitations of the current processing technology, the structure of this method is relatively complicated and it is generally suitable for the lower operating frequency band. Second, the method of loading lumped elements is adopted to reduce the size of the structure [22], [23]. Since the high-frequency lumped inductor and capacitor components are very expensive and have parasitic elements, this scheme is also constrained. Third, many groups focus on the research of 2.5-D and 3-D FSS, which can improve the angular stability by extending the structure along the longitudinal direction [24]–[26]. Unfortunately, 2.5-D or 3-D FSS structures require a much thicker space and higher complexity, which is inappropriate in some application scenarios. At the same time, the most serious problem is that the angular instability is still existing for TM mode, although the proposed miniaturized structure is insensitive to the incident angle for TE mode [27], [28].

In this article, a novel miniaturized concept of strong-coupled FSS (SC-FSS) based on the interlayer coupling is developed to achieve the excellent angular stability for both TE and TM modes. First, we introduce the concept and theory of SC-FSS by designing a conceptual model in Section II. Its field and surface current distributions are investigated, and a corresponding equivalent circuit model (ECM) is also established to explain its operating principle. In addition, we discuss the advantages of this miniaturization strategy. Furthermore, to verify this concept, an almost all-angle-insensitive band-stop SC-FSS structure for both TE and TM modes is presented and fabricated in Section III. The angle-independent property of this structure is consistent with the simulated results by CST and ECM, which validates the proposed technique. Finally, a brief conclusion is drawn in Section IV.

II. CONCEPT AND THEORY OF SC-FSS

A. Structure Description of the Conceptual Model

Fig. 1(a) shows a conceptual design of an SC-FSS, which consists of three layers, wherein the two metal layers are separately attached on both sides of a thin dielectric layer D_0 . As shown in Fig. 1(b), the top layer contains a circular patch A_1 connected

Manuscript received May 26, 2020; revised July 23, 2020; accepted August 15, 2020. Date of publication September 7, 2020; date of current version February 17, 2021. This work was supported by the Zhejiang Laboratory Foundation of China under Grant 2020KCDAB01. (Corresponding author: Erping Li.)

Tianwu Li, Yudi Fan, and Erping Li are with the Key Laboratory of Advanced Micro-Nano Electronic Devices and Smart Systems and Applications, College of Information Science and Electronic Engineering, Zhejiang University, Hangzhou 310027, China, and also with Zhejiang University–University of Illinois at Urbana-Champaign Institute, Zhejiang University, Haining 314400, China (e-mail: litianwu@zju.edu.cn; woodyfan@zju.edu.cn; liep@zju.edu.cn).

Da Li is with the 14th Research Institute, China Electronics Technology Group Co., Nanjing 225411, China (e-mail: li-da@zju.edu.cn).

Pengfei Qin, Yijie Gu, Panpan Zuo, and Wei E. I. Sha are with the Key Laboratory of Advanced Micro-Nano Electronic Devices and Smart Systems and Applications, College of Information Science and Electronic Engineering, Zhejiang University, Hangzhou 310027, China (e-mail: qinpf@zju.edu.cn; ygu@zju.edu.cn; kldpp19880608@126.com; weisha@zju.edu.cn).

Color versions of one or more of the figures in this article are available online at <https://ieeexplore.ieee.org>.

Digital Object Identifier 10.1109/TEM.2020.3018558

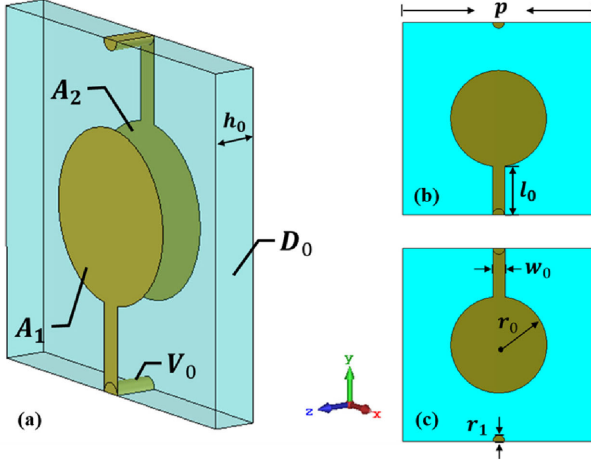


Fig. 1. Schematic view of the proposed SC-FSS conceptual model. (a) 3-D view. (b) Top view. (c) Bottom view.

TABLE I
PHYSICAL DIMENSIONS OF THE PROPOSED SC-FSS CONCEPTUAL MODEL

Parameter	p	h_0	r_0	r_1	w_0
Value (mm)	10	0.254	2	0.15	0.3

with a metal strip, while the geometry of the bottom layer is the same as that of the top one but mirror symmetry in Fig. 1(c). In addition, at the edge of the unit cell, the top and bottom layers are connected through the metal vias V_0 , which ensures that the top and bottom metal strips of adjacent units are connected together. Rogers RT5880 with permittivity $\epsilon_r = 2.2$ and tangent loss $\tan \delta = 0.0009$ is used as the material of the dielectric layer. The optimized geometric parameters are displayed in Table I.

Full-wave simulations are implemented using the electromagnetic simulation software CST Microwave Studio for TE mode under different incident angles (0° – 88° , step = 2°), where the boundaries in the x and y direction are set as *unit cell* and those in the z -direction are set as *open (add space)*. And the *frequency-domain solver* is chosen to calculate. In order to observe the angle response of this model more clearly, the transmission spectrum of the proposed SC-FSS conceptual model is drawn by those results as presented in Fig. 2, wherein there is a stopband near 2.35 GHz. Interestingly, it can be clearly found that at the resonant frequency $f_s(\theta)$, the structure is not sensitive to the incident angles, even when the angle approaches at 90° .

B. Operation Principle

The ECM is the most intuitive way to analyze the transmission performance of the structure, which can help us understand the working principle of the structure and guide us to design the specific structure. To further investigate the working principle of the structure, we first consider a traditional dipole-type FSS structure, as shown in Fig. 3(a). Its distributions of the electric field and surface current at the resonant frequency are displayed in Fig. 3(c) and (d), wherein the surface current distributes on the patch that can be equivalent to inductance L_0 . Meanwhile,

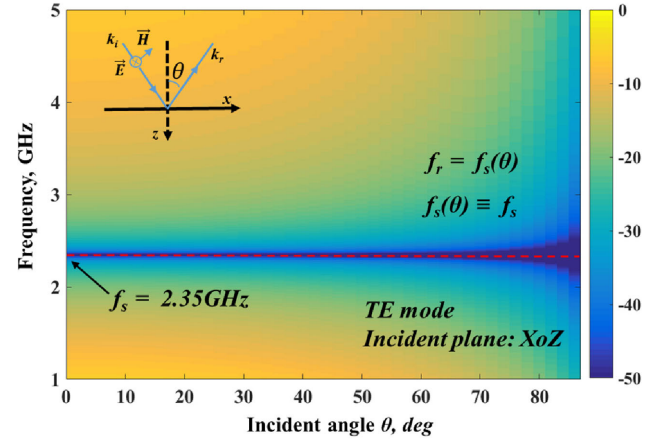


Fig. 2. Transmission spectrum of the proposed SC-FSS conceptual model for TE mode.

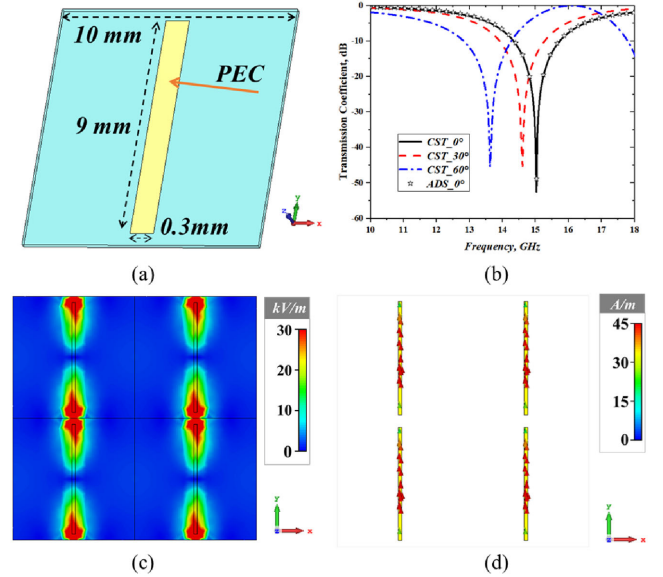


Fig. 3. (a) Schematic view of a dipole-type FSS. (b) Frequency response of the dipole-type FSS under different incident angles for TE mode. (c) Distributions of the electric field at the resonant frequency. (d) Distributions of the surface current at the resonant frequency (15 GHz).

the electric field concentrates on the truncation at the two ends of the adjacent patches generating a capacitance C_0 . They form an *LC* series resonance with a stopband at the resonance frequency $f_{s0} = 1/(2\pi\sqrt{L_0C_0})$. Based on the research in [7], we calculate the inductance $L_0 = 7.36$ nH and the capacitance $C_0 = 15.25$ fF from the structure parameters. In addition, due to the coupling between the unit cells, there will be an angular dispersion [29], as depicted in Fig. 3(b) that the resonance frequency is shifted at the oblique incidence.

Different from the traditional FSS design, the SC-FSS benefits from the strong coupling between the top and bottom layers. To further understand and analyze the physical mechanism, there are the distributions of the electric field (in the middle of the dielectric layer) at 2.35 GHz under TE mode, as shown in

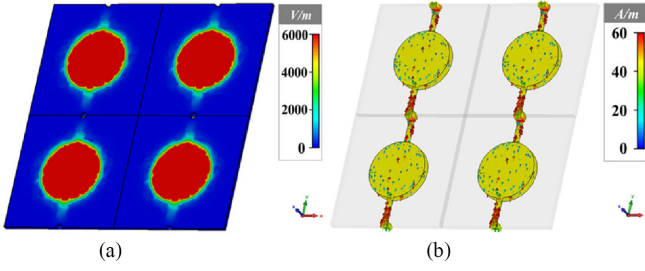


Fig. 4. Distributions of the electric field and surface current at 2.35 GHz for TE mode. (a) Electric field distributions. (b) Surface current distributions.

Fig. 4(a). The electric field is completely bound between two circular patches A_1 and A_2 , forming a strong coupling in the z -direction at the resonance frequency. With the effect of the dielectric layer, the two circular patches A_1 and A_2 can be regarded as the parallel plate capacitance C_s at the specific frequency, when the incident electromagnetic waves reach the surface of the structure. Compared with the traditional dipole-type FSS structure presented in Fig. 3, this parallel plate capacitance C_s (1.115 pF) is bigger than the capacitance C_0 (15.25 fF) generated at the two ends of the adjacent patches, which is extremely advantageous for miniaturizing the structure. Thus, under the same unit cell size, the resonant frequency of SC-FSS (2.35 GHz) is much smaller than that of the traditional dipole FSS (15 GHz).

At the same time, it can be found that the currents mainly distribute on the strip and vias [see Fig. 4(b)], which is equivalent to an inductance L_0 , and the vias are considered to be the inductance L_v . The ECM is shown in Fig. 5(b), where the equivalent capacitance C_s and inductance L_s form an LC series resonance with a stopband at this resonant frequency f_s . In order to better verify the above-mentioned theoretical analysis, the parameters are extracted and calculated by the following empirical formulae based on the research in [4] and [30]:

$$C_s = \frac{\varepsilon_0 \varepsilon_r \pi R_e^2}{h_0} \quad (1)$$

$$R_e = r_0 \left(1 + \frac{2h_0}{\pi r_0 \varepsilon_r} \left(\ln \left(\frac{\pi r_0}{2h_0} \right) + 1.7726 \right) \right)^{1/2} \quad (2)$$

$$L_0 = \mu_0 \frac{p - 2R_e - (\pi - 2)r_1}{2\pi} \ln \left(\frac{2(p - 2R_e - (\pi - 2)r_1)}{w_0} \right) \quad (3)$$

$$L_v = \frac{h_0}{5} \left(1 + \ln \left(\frac{2h_0}{r_1} \right) \right) \quad (4)$$

$$L_s = L_0 + L_v. \quad (5)$$

To consider the fringing effect of the E -field, a correction factor R_e in (2) given by [31] is introduced to obtain the accurate capacitance value. Conventionally, due to the angular dispersion of traditional structures, which makes the equivalent circuit parameters change with the incident angles, the ECM can only characterize the transmission response at the normal incidence.

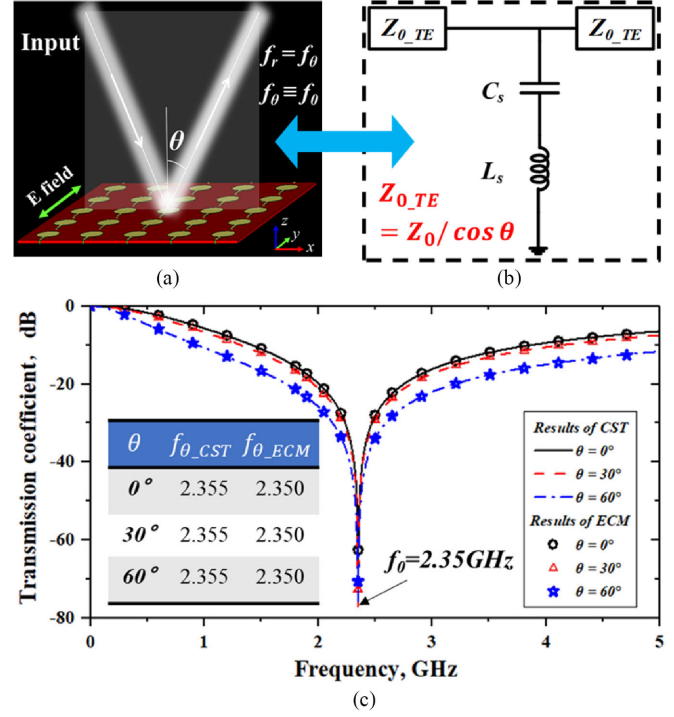


Fig. 5. (a) Schematic view of the proposed SC-FSS at oblique incidences. (b) ECM. (c) Simulation results of ECM in comparison with those by CST. Calculated LC parameters are $C_s = 1.115$ pF and $L_s = 4.098$ nH.

What is more surprising is that the ECM of the proposed SC-FSS can fully depict the transmission at all incident angles for TE mode because the designed structure is insensitive to all incident angles based on the above-mentioned principle analysis, which means that the equivalent circuit parameters are not affected by the incident angle. The equivalent circuit is simulated by the circuit simulation software ADS. For TE mode, the free-space impedance of the incident waves varies with $Z_0/\cos(\theta)$, while it changes to $Z_0 \cdot \cos(\theta)$ for TM mode [2].

Therefore, we can simulate the transmission curves for the oblique incidence by adjusting the input and output impedances in the equivalent circuit, and the comparison results obtained by CST are shown in Fig. 5(c), where the error of resonant frequency calculated by ECM is less than 0.2% compared with that obtained by CST. For the same incident angle, the transmission curves simulated by ECM are completely consistent with those obtained by CST, confirming that the equivalent circuit parameters are independent of the incident angle, which means the proposed SC-FSS conceptual model is insensitive to all incident angles for TE mode. As a result, the equivalent inductance L_s and capacitance C_s under different structural parameters can be derived by the numerical calculation, and the corresponding transmission curve can be demonstrated by ADS. This computational efficiency is faster than the full-wave simulation software, which can improve the efficiency of design and development.

Furthermore, it must be emphasized that adding vias is a necessary condition in the SC-FSS design. Those vias connect all elements together, which ensures the interlayer coupling can

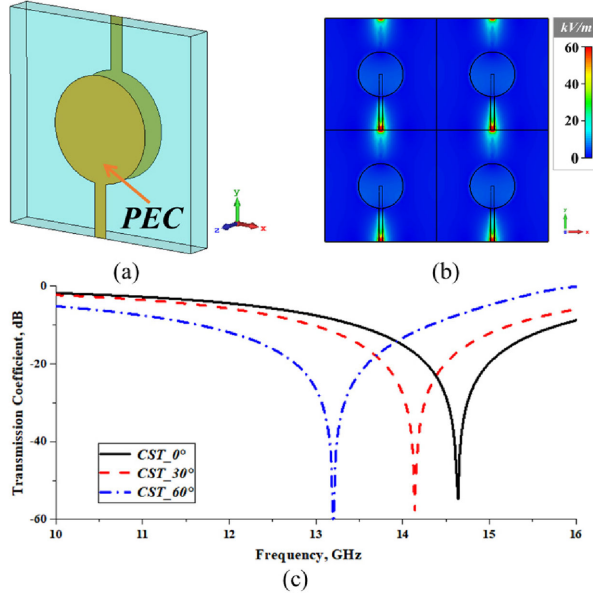


Fig. 6. (a) Similar structure to the structure in Fig. 1(a) without via at the edge of the unit cell. (b) Distributions of electric field at 14.6 GHz for TE mode. (c) Performance under oblique incidence for TE mode.

be excited and there will be no coupling between different unit cells. Disconnecting the top with the bottom layers by removing the via will change the resonant mechanism, where the electric field distributes at the truncation of the cell boundary, instead of the two circular patches [see Fig. 6(b)]. Fig. 6(c) describes the situation without vias, where the resonance occurs at 14.6 GHz, which is much higher than the resonance with vias at 2.35 GHz. Unfortunately, this will lead to the coupling between the elements and the structure is sensitive to the incident angles, as shown in Fig. 6(c).

C. Advantages of SC-FSS in Miniaturization

SC-FSS provides multidimensional adjustment in the miniaturization design. First, the bigger the relative area is, the stronger the coupling will be. Thus, the radius r_0 of a circular patch adjusts the miniaturization of the structure. Second, compared with the traditional FSS structure, the dielectric of SC-FSS will have a greater function, as its thickness h_0 and permittivity ϵ_r directly affect this interlayer coupling. The effects of the above-mentioned factors on the miniaturization of SC-FSS are described in Table II. It can be observed that the thinner the dielectric thickness is, the higher miniaturization will be, which is one of the very meaningful advantages of this miniaturized method. Besides, higher permittivity ϵ_r will lead to a stronger coupling. As a result, SC-FSS can achieve a very high degree of miniaturization in theory. In addition to the angular stability, it is also significant to solve the EMI problem of the chip and package in a narrow space. Furthermore, besides the miniaturization, we mainly solve the angular dispersion by eliminating the coupling between the elements. Fig. 7 shows that the proposed SC-FSS has good angular stability under different miniaturization levels

TABLE II
EFFECTS OF THE STRUCTURAL PARAMETERS ON THE MINIATURIZATION OF SC-FSS

Case	r_0 (mm)	h_0 (mm)	ϵ_r	Resonant frequency	Unit cell size
①	2.2	0.2	2.2	1.92 GHz	$0.064 \lambda_0$
②	1.4	0.2	2.2	2.64 GHz	$0.088 \lambda_0$
③	3	0.2	2.2	1.66 GHz	$0.055 \lambda_0$
④	2.2	0.1	2.2	1.38 GHz	$0.046 \lambda_0$
⑤	2.2	0.3	2.2	2.32 GHz	$0.077 \lambda_0$
⑥	2.2	0.2	3.3	1.60 GHz	$0.053 \lambda_0$
⑦	2.2	0.2	6.5	1.14 GHz	$0.038 \lambda_0$
⑧	3	0.1	10	0.56 GHz	$0.018 \lambda_0$

Cases ①②③ show the effect of the radius of circular patch r_0 .

Cases ④⑤ show the effect of the thickness of dielectric h_0 .

Cases ⑥⑦ show the effect of relative permittivity ϵ_r .

Case ⑧ proves that we can further miniaturize the structure size to 0.018λ and even smaller by adjusting these parameters.

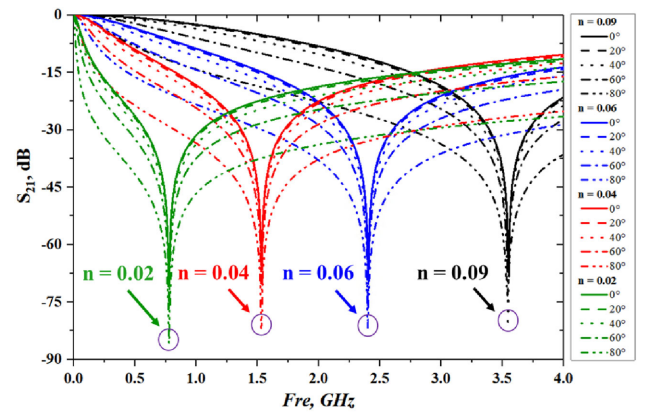


Fig. 7. Angular response of the SC-FSS structure under different miniaturization levels. $n = P/\lambda$, where the parameter “ n ” means the miniaturization level, P is the unit cell size (8 mm), and λ is the wavelength of the corresponding operating frequency.

for TE mode, which makes it possible to design the FSS structure insensitive to the incident angle at a higher frequency.

III. DUAL-POLARIZATION BAND-STOP SC-FSS STRUCTURE

A. Structure Description and Operation Principle

In practical applications, due to the complex electromagnetic environment, the designed SC-FSS structure is often required to have good polarization stability. However, in general, the angle problem is more prominent for TM mode, because the vector components of the electric field will change accordingly, as the incident angle increases. Consequently, how to solve this problem and realize a dual-polarized stable structure insensitive to the incident angle becomes a big challenge.

As analyzed in the previous study [4], the more miniaturized the unit cell size, the better the angle stability. In order to solve

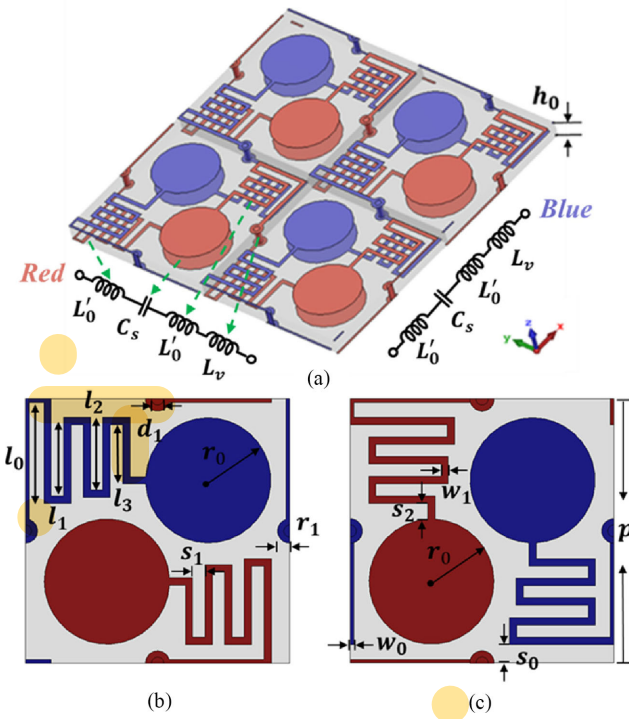


Fig. 8. Structure of the stopband SC-FSS for dual polarizations. (a) 3-D view. (b) Top view. (c) Bottom view. Optimized geometric parameters are $p = 4.3$ mm, $h_0 = 0.254$ mm, $\epsilon_r = 6.5$, $r_0 = 1.02$ mm, $d_1 = 0.2$ mm, $r_1 = 0.2$ mm, $w_0 = 0.06$ mm, $w_1 = 0.12$ mm, $s_0 = 0.3$ mm, $s_1 = 0.2$ mm, $s_2 = 0.26$ mm, $l_0 = 1.52$ mm, $l_1 = 1.28$ mm, $l_2 = 1.18$ mm, and $l_3 = 0.96$ mm.

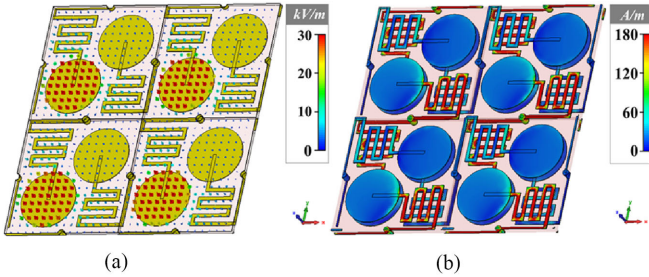


Fig. 9. Distributions of surface current and electric field at 2 GHz under TE polarization incidence. (a) Electric field distributions. (b) Surface current distributions.

the incident angle problem for TM mode, we design a more compact SC-FSS structure, as shown in Fig. 8. In addition to the strong coupling between different layers, the structure also introduces the meandered inductance, which further improves the miniaturization of the designed structure.

The red parts of the structure can control the incident y-polarization waves, while the x-polarization waves are regulated by the blue parts. The surface currents and electric field distributions of the proposed SC-FSS array at 2 GHz for TE mode are shown in Fig. 9. It can be observed that the electric field is mainly concentrated between the red circular patches at this time and the current is mainly distributed on the red strips. On the other hand, they are mainly distributed on the blue parts for the TM mode.

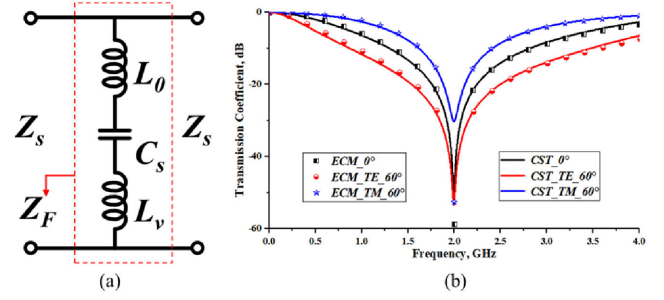


Fig. 10. (a) Proposed ECM, where Z_F is the equivalent impedance of the FSS structure and Z_s is the free-space impedance of the incident waves. (b) Simulation results of ECM in comparison with those by CST.

The ECM of this structure is the same as the single-polarization structure in Section II, as shown in Fig. 10(a). Through the formulae (1)–(5), we can calculate the equivalent capacitance $C_s = 1$ pF and inductance $L_s = 6.35$ nH.

The circuit simulation results obtained by the circuit simulation software ADS are compared with the full-wave simulation results, as shown in Fig. 10(b), where the simulation results of CST and ADS agree with each other, which verifies that the above-mentioned analysis is practicable. It should be noted that the peak value is varying as the incident angle and polarization. This is the result that the free-space impedance of the incident waves Z_s varies with $Z_0/\cos(\theta)$ for TE mode, while it changes to $Z_0 \cdot \cos(\theta)$ for TM mode, where $Z_0 = E/H = 377 \Omega$

$$S_{11} = \frac{Z_s - Z_{in}}{Z_s + Z_{in}} \quad (6)$$

$$Z_{in} = \frac{Z_F \cdot Z_s}{Z_F + Z_s} \quad (7)$$

From formulae (6) and (7), the reflection coefficients S_{11} at the oblique incidence can be expressed as

$$S_{11} = \frac{1}{1 + 2 \frac{Z_F \cos(\theta)}{Z_0}}, \text{ for TE mode} \quad (8)$$

$$S_{11} = \frac{1}{1 + 2 \frac{Z_F}{Z_0 \cos(\theta)}}, \text{ for TM mode.} \quad (9)$$

For a certain frequency, Z_F is a constant. For TE mode, the reflection coefficient S_{11} will increase, while it decreases for TM mode, which is consistent with the simulation results.

Furthermore, the transmission spectra of the proposed stopband SC-FSS structure under different polarizations and incident angles are shown in Fig. 11. Obviously, when the incident angle changes from 0° to 88° , the resonance frequencies of SC-FSS remain at f_s all the time for both TE and TM modes.

B. Implementation and Experimental Verification

Finally, the prototype is fabricated by the printed circuit board (PCB) technology to verify the feasibility of the proposed structure, as shown in Fig. 12(b). It consists of 98×63 unit cells with a board size of 430×285 mm. It was measured by the free-space method. The entire testing process is carried out in a microwave anechoic chamber to reduce the EMI effects in the environment.

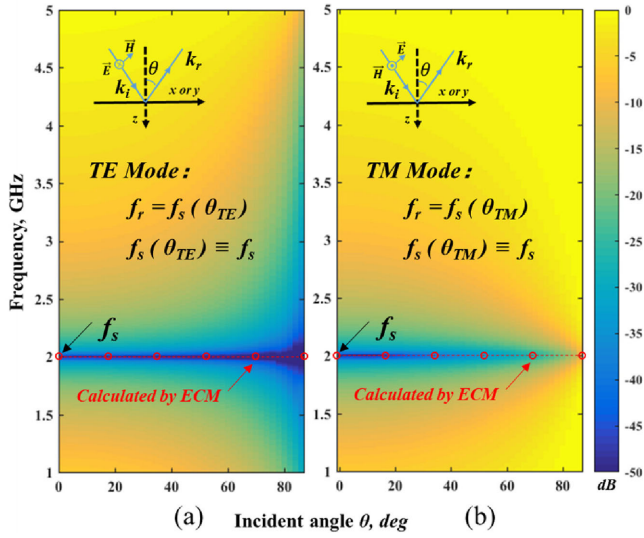


Fig. 11. Transmission spectra of the proposed stopband SC-FSS structure under different incident angles. (a) TE mode. (b) TM mode.

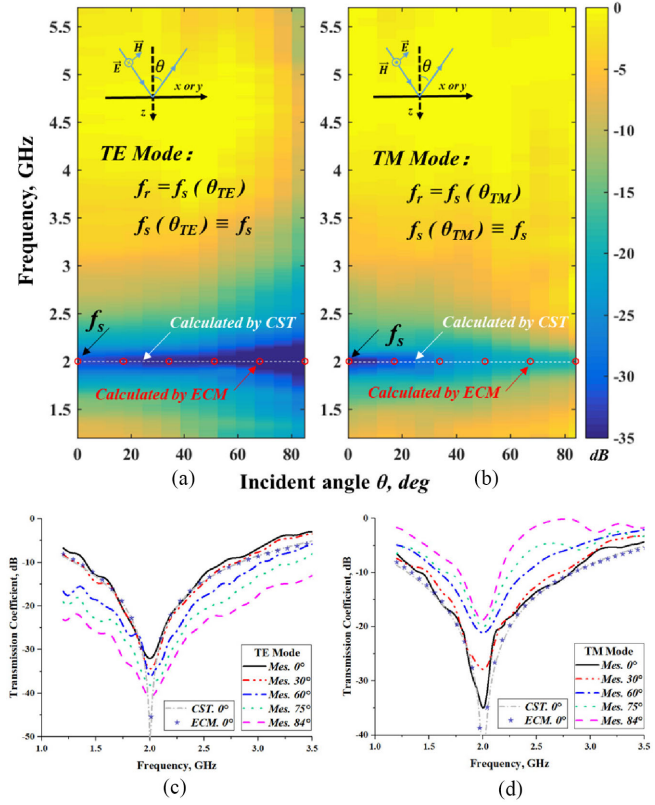


Fig. 13. Measured results of the proposed SC-FSS structure and the comparison with those by CST and ECM. (a) and (c) TE mode. (b) and (d) TM mode.

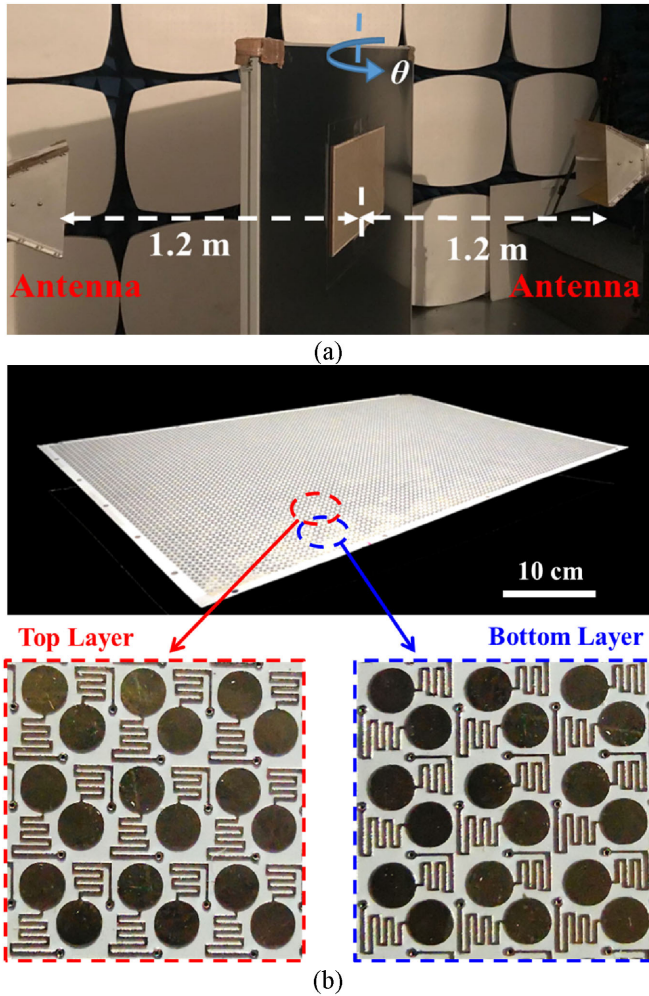


Fig. 12. (a) Photograph of the FSS measured in a microwave anechoic chamber. (b) Photograph of the fabricated FSS.

The experimental setup is shown in Fig. 12(a), where a pair of horn Antennas HD-10180 and a vector network analyzer ZVA67 were employed for testing. For each incident angle, we measure two sets of data separately. Data₁ is the environmental reference value measured without loading FSS, while Data₂ is the measured value with loading FSS. The transmission coefficient of the prototype, S_{21} , is equal to Data₂ minus Data₁. Fig. 13 shows the transmission responses under different incident angles for TE and TM modes, respectively. The transmission zeros are always stable at 2 GHz under the variety of incident angle (0° – 75° , step = 7.5° and 84°) for both TE and TM modes, which is consistent with the results of ECM and full-wave simulation. For the normal incidence, the stopband bandwidth of -10 dB is over 1.28 GHz. As the free impedance of the incident waves changes at the oblique incidence, the stopband bandwidth of TE mode will enlarge with the increase of incident angles, while the bandwidth narrows for TM mode. Furthermore, to further confirm the superiority of the proposed method, a performance comparison of previously angular stability and miniaturized FSS designs with the proposed structure in this article is listed in Table III. It is concluded that no work in the existing pieces of literature has realized the performance that the resonance frequency is insensitive to almost all incident angles for both TE and TM modes, and the SC-FSS structure has the more miniaturized unit cell in contrast with other similar works. As a

TABLE III
CHARACTERISTICS OF DIFFERENT FSS DESIGNS

FSS designs	Resonance frequency	Unit cell	Angular stability	Resonance frequency Max. deviation (%)
Structure in [28]	1.89 GHz	10 mm 0.063 λ	45°	TE: Unchanged TM: Blue shift about 7.4%
Structure in [31]	7.4 GHz	8 mm 0.19 λ	80°	TE: Blue shift about 4.6% TM: Blue shift about 4.0%
Structure in [20]	3.3 GHz	6.3 mm 0.069 λ	80°	TE: Red shift about 1.2% TM: Blue shift about 1.81%
Structure in Fig. 8	2 GHz	4.3 mm 0.0286 λ	84°	Unchanged for both TE and TM Modes

result, it can be applied to solve the problem of EMI in a narrow space with a large incident angle.

IV. CONCLUSION

The miniaturized concept of SC-FSS, which is insensitive to almost all incident angles, is proposed in this article. First, we introduce the concept and analyze the working principle of the SC-FSS conceptual model. Then the advantages of SC-FSS in miniaturization are discussed. Furthermore, in order to verify this design concept, especially to solve the angle-sensitive problem for TM mode, a dual-polarized stopband SC-FSS structure is designed and presented, whose transmission zeros are always maintained at 2 GHz even when the angle changes to 84° for both TE and TM modes in the measurement results. In conclusion, the proposed SC-FSS is a good miniaturized method with excellent angular stability, which can be well applied to the antenna reflectors and complex EMI shielding in a narrow space.

REFERENCES

- [1] T. K. Wu, *Frequency Selective Surface and Grid Array*. New York, NY, USA: Wiley, 1995.
- [2] B. A. Munk, *Frequency Selective Surfaces: Theory and Design*. New York, NY, USA: Wiley, 2000.
- [3] Y. Shang, Z. Shen, and S. Xiao, "Frequency-selective rasorber based on square-loop and cross-dipole arrays," *IEEE Trans. Antennas Propag.*, vol. 62, no. 11, pp. 5581–5589, Nov. 2014.
- [4] D. Li, T.-W. Li, E.-P. Li, and Y.-J. Zhang, "A 2.5-D angularly stable frequency selective surface using via-based structure for 5G EMI shielding," *IEEE Trans. Electromagn. Compat.*, vol. 60, no. 3, pp. 768–775, Jun. 2018.
- [5] L. Alonso-Gonzalez, S. Ver-Hoeve, M. Fernandez-Garcia, and F. L. H. Andres, "Layer-to-layer angle interlock 3D woven bandstop frequency selective surface," *Prog. Electromagn. Res.*, vol. 162, pp. 81–94, 2018.
- [6] T. Li, D. Li, L. Zhou, and E. Li, "A miniaturised FSS structure with excellent angular stability based on strong coupling for millimeter-wave communication," *Electron. Lett.*, vol. 54, no. 8, pp. 511–513, Apr. 2018.
- [7] D. Li *et al.*, "A low-profile broadband bandpass frequency selective surface with two rapid band edges for 5G near-field applications," *IEEE Trans. Electromagn. Compat.*, vol. 59, no. 2, pp. 670–676, Apr. 2017.
- [8] R. Sivasamy, L. Murugasamy, M. Kanagasabai, E. F. Sundarsingh, and M. G. N. Alsath, "A low-profile paper substrate-based dual-band FSS for GSM shielding," *IEEE Trans. Electromagn. Compat.*, vol. 58, no. 2, pp. 611–614, Apr. 2016.
- [9] I. S. Syed, Y. Ranga, L. Matekovits, K. P. Esselle, and S. G. Hay, "A single-layer frequency-selective surface for ultrawideband electromagnetic shielding," *IEEE Trans. Electromagn. Compat.*, vol. 56, no. 6, pp. 1404–1411, Dec. 2014.
- [10] Z. L. Wang, K. Hashimoto, N. Shinohara, and H. Matsumoto, "Frequency-selective surface for microwave power transmission," *IEEE Trans. Microw. Theory Techn.*, vol. 47, no. 10, pp. 2039–2042, Oct. 1999.
- [11] B. Schoenlinner, A. Abbaspour-Tamijani, L. C. Kempel, G. M. Rebeiz, "Switchable low-loss RF MEMS Ka-band frequency-selective surface," *IEEE Trans. Microw. Theory Techn.*, vol. 52, no. 11, pp. 2474–2481, Nov. 2004.
- [12] N. Behdad, M. Al-Joumayly, and M. Salehi, "A low-profile third-order bandpass frequency selective surface," *IEEE Trans. Antennas Propag.*, vol. 57, no. 2, pp. 460–466, Feb. 2009.
- [13] M. Yan *et al.*, "A tri-band, highly selective, bandpass FSS using cascaded multilayer loop arrays," *IEEE Trans. Antennas Propag.*, vol. 64, no. 5, pp. 2046–2049, May 2016.
- [14] A. Abbaspour-Tamijani, K. Sarabandi, and G. M. Rebeiz, "Antenna-filter-antenna arrays as a class of bandpass frequency-selective surfaces," *IEEE Trans. Microw. Theory Techn.*, vol. 52, no. 8, pp. 1781–1789, Aug. 2004.
- [15] K. Payne, K. Xu, and J. H. Choi, "Generalized synthesized technique for the design of thickness customizable high-order bandpass frequency-selective surface," *IEEE Trans. Microw. Theory Techn.*, vol. 66, no. 11, pp. 4783–4793, Nov. 2018.
- [16] G. Q. Luo, W. Hong, Q. H. Lai, K. Wu, and L. L. Sun, "Design and experimental verification of compact frequency-selective surface with quasi-elliptic bandpass response," *IEEE Trans. Microw. Theory Techn.*, vol. 55, no. 12, pp. 2481–2487, Dec. 2007.
- [17] M. N. Hussein, J. Zhou, Y. Huang, M. Kod, and A. P. Sohrab, "A miniaturized low-profile multilayer frequency-selective surface insensitive to surrounding dielectric materials," *IEEE Trans. Microw. Theory Techn.*, vol. 65, no. 12, pp. 4851–4860, Dec. 2017.
- [18] X. Liu, Q. Wang, W. Zhang, M. Jin, and M. Bai, "On the improvement of angular stability of the 2nd-order miniaturized FSS structure," *IEEE Antennas Wireless Propag. Lett.*, vol. 15, pp. 826–829, 2016.
- [19] P.-C. Zhao, Z.-Y. Zong, W. Wu, B. Li, and D.-G. Fang, "An FSS structure with geometrically separable meander-line inductors and parallel-plate capacitors," *IEEE Trans. Antennas Propag.*, vol. 65, no. 9, pp. 4693–4705, Sep. 2017.
- [20] S. N. Azemi, K. Ghorbani, and W. S. T. Rowe, "Angularly stable frequency selective surface with miniaturized unit cell," *IEEE Microw. Wireless Compon. Lett.*, vol. 25, no. 7, pp. 454–456, Jul. 2015.
- [21] S. Ghosh and K. V. Srivastava, "An angularly stable dual-band FSS with closely spaced resonances using miniaturized unit cell," *IEEE Microw. Wireless Compon. Lett.*, vol. 27, no. 3, pp. 218–220, Mar. 2017.
- [22] H. L. Liu, K. L. Ford, and R. J. Langley, "Design methodology for a miniaturized frequency selective surface using lumped reactive components," *IEEE Trans. Antennas Propag.*, vol. 57, no. 9, pp. 2732–2738, Sep. 2009.
- [23] R.-R. Xu, H.-C. Zhao, Z.-Y. Zong, and W. Wu, "Dual-band capacitive loaded frequency selective surfaces with close band spacing," *IEEE Microw. Wireless Compon. Lett.*, vol. 18, no. 12, pp. 782–784, Dec. 2008.
- [24] Z. Shen, J. Wang, and B. Li, "3-D frequency selective rasorber: Concept, analysis, and design," *IEEE Trans. Microw. Theory Techn.*, vol. 64, no. 10, pp. 3087–3096, Oct. 2016.
- [25] T. Deng, Y. Yu, Z. Shen, and Z. N. Chen, "Design of 3-D multilayer ferrite-loaded frequency-selective rasorbers with wide absorption bands," *IEEE Trans. Microw. Theory Techn.*, vol. 67, no. 1, pp. 108–117, Jan. 2019.
- [26] D. Li, T. Li, and E. Li, "Implementation of ultra-miniaturised frequency-selective structures based on 2.5D convoluted segments," *Electron. Lett.*, vol. 54, no. 8, pp. 476–478, Apr. 2018.
- [27] Z. Zhao, J. Li, H. Shi, X. Chen, and A. Zhang, "A low-profile angle-insensitive bandpass frequency-selective surface based on vias," *IEEE Microw. Wireless Compon. Lett.*, vol. 28, no. 3, pp. 200–202, Mar. 2018.
- [28] T. Hussain, Q. Cao, J. K. Kayani, and I. Majid, "Miniaturization of frequency selective surfaces using 2.5-D knitted structures: Design and synthesis," *IEEE Trans. Antennas Propag.*, vol. 65, no. 5, pp. 2405–2412, May 2017.
- [29] M. Qiu, M. Jia, S. Ma, S. Sun, Q. He, and L. Zhou, "Angular dispersions in terahertz metasurfaces: Physics and applications," *Phys. Rev. Appl.*, vol. 9, 2018, Art. no. 054050.
- [30] H. Johnson and M. Graham, *High-Speed Signal Propagation: Advanced Black Magic*. Upper Saddle River, NJ, USA: Prentice-Hall, 2003.
- [31] L. Shen, S. Long, M. Allering, and M. Walton, "Resonant frequency of a circular disc, printed-circuit antenna," *IEEE Trans. Antennas Propag.*, vol. 25, no. 4, pp. 595–596, Jul. 1977.
- [32] G. S. Paul and K. Mandal, "Polarization-insensitive and angularly stable compact ultrawide stop-band frequency selective surface," *IEEE Antennas Wireless Propag. Lett.*, vol. 18, no. 9, pp. 1917–1921, Sep. 2019.



Tianwu Li received the B.S. degree in communication engineering from the School of Mechanical, Electrical and Information Engineering, Shandong University, Jinan, China, in 2016. He is currently working toward the Ph.D. degree in electronics science and technology from Zhejiang University, Hangzhou, China.

His current research interests focus on frequency selective surface, metamaterial, metasurface, and EMC/EMI design in the communication system and chip.



Da Li received the B.S. and Ph.D. degrees in electrical engineering from Zhejiang University, Hangzhou, China, in 2014 and 2019, respectively.

In 2017, he joined Nanyang Technological University, Singapore, as a Project Researcher. He is currently with 14th Research Institute, China Electronics Technology Group Company, Nanjing, China. His current research interests include 5G antenna arrays, frequency-selective structures, and electromagnetic compatibility.



Pengfei Qin received the B.S. and Ph.D. degrees in electrical engineering from Zhejiang University, Hangzhou, China, in 2014 and 2020, respectively.

In April 2018, he was a Visiting Student with the Singapore University of Technology and Design, Singapore, for four months.

His current research interests focus on metamaterials, metasurfaces, and spoof surface plasmons.



Yudi Fan received the B.Eng. degree in the field of informance and communication engineering in 2019 from the College of Information Science and Electronic Engineering, Zhejiang University, Zhejiang, China, where he is currently working toward Ph.D. degree in electronics science and technology.

His current research interests focus on absorber, metamaterials, and metasurfaces.



Yijie Gu received the B.Eng. degree in electronics science and technology in 2017 from the College of Information Science and Electronic Engineering, Zhejiang University, Zhejiang, China, where he is currently working toward Ph.D. degree in electronics science and technology.

His current research interests focus on spoof surface plasmons, metamaterials, and metasurfaces.



Panpan Zuo (Member, IEEE) was born in Tai'an, China, in 1988. She received the B.S. degree from Inner Mongolia University, Hohhot, China, in 2010, and the Ph.D. degree from the Hebei University of Technology, Tianjin, China, in 2020, both in electrical engineering.

Her current research interests include electrical modeling and the design of 3-D electronic packages, signal integrity, and power integrity in high-speed packages.



Wei E. I. Sha (Senior Member, IEEE) received the B.S. and Ph.D. degrees in electronic engineering from Anhui University, Hefei, China, in 2003 and 2008, respectively.

From July 2008 to July 2017, he was a Postdoctoral Research Fellow and then a Research Assistant Professor with the Department of Electrical and Electronic Engineering, University of Hong Kong, Hong Kong. From March 2018 to March 2019, he was with University College London as a Marie Skłodowska-Curie Individual Fellow. In October 2017, he joined

the College of Information Science and Electronic Engineering, Zhejiang University, Hangzhou, China, where he is currently a tenure-tracked Assistant Professor. His research involves the fundamental and applied aspects in the computational and applied electromagnetics, nonlinear and quantum electromagnetics, micro- and nano-optics, optoelectronic device simulation, and multiphysics modeling. He has authored or coauthored 136 refereed journal papers, 121 conference publications (including 31 invited talks), five book chapters, and two books. His Google Scholar citation is 5378 with the h-index of 34. He served as a Reviewer for 50 technical journals and Technical Program Committee member of nine IEEE conferences. His research interests include theoretical and computational research in electromagnetics and optics, focusing on the multiphysics and interdisciplinary research.

Dr. Sha is a member of OSA. He was an Associate Editor for the Progress in Electromagnetics Research, IEEE ACCESS, and IEEE OPEN JOURNAL OF ANTENNAS AND PROPAGATION, and the Guest Editor for the IEEE JOURNAL ON MULTISCALE AND MULTIPHYSICS COMPUTATIONAL TECHNIQUES AND THE APPLIED COMPUTATIONAL ELECTROMAGNETICS SOCIETY JOURNAL. He was a recipient of the Second Prize of Science and Technology from Anhui Province Government, China, in 2015, Thousand Talents Program for Distinguished Young Scholars of China, in 2017, five Best Student Paper Prizes, and one Young Scientist Award with his students.



Erping Li (Fellow, IEEE) received the Ph.D. degree in electrical engineering from Sheffield Hallam University, Sheffield, U.K., in 1992.

Since 1989, he has been a Research Fellow, Principal Research Engineer, Associate Professor, and the Technical Director with the National University of Singapore. In 2000, he joined the A*STAR Research Institute of High Performance Computing, Singapore, as a Principal Scientist and Director. He is currently a Changjiang-Qianren Distinguished Professor with the Department of Information Science and Electronic Engineering, Zhejiang University, Hangzhou, China; Dean of the Joint Institute of Zhejiang University–University of Illinois at Urbana-Champaign, Zhejiang University, Hangzhou, China. He has been a General Chair and Technical Chair for many international conferences. He was the President for the 2006 International Zurich Symposium on EMC, the Founding General Chair for Asia-Pacific EMC Symposium, General Chair for 2008, 2010, 2012, and 2016 APEMC, and 2010 IEEE Symposium on Electrical Design for Advanced Packaging Systems. He has been invited to give numerous invited talks and plenary speeches at various international conferences and forums. His current research interests include electrical modeling and design of micro/nanoscale integrated circuits, 3-D electronic package integration, and nanoplasmonic technology.

Prof. Li is a Fellow of MIT Electromagnetics Academy, USA. He is the recipient of the 2015 IEEE Richard Stoddard Award on EMC, IEEE EMC Technical Achievement Award, Singapore IES Prestigious Engineering Achievement Award, and Changjiang Chair Professorship Award from the Ministry of Education in China, and a number of Best Paper Awards. He was elected to the IEEE EMC Distinguished Lecturer in 2007. From 2006–2008, he was an Associate Editor for the IEEE MICROWAVE AND WIRELESS COMPONENTS LETTERS, Guest Editor for 2006 and 2010 IEEE TRANSACTIONS ON EMC SPECIAL ISSUES, Guest Editor for 2010 IEEE TRANSACTIONS ON MTT APMC SPECIAL ISSUE, and is currently an Associate Editor for the IEEE TRANSACTIONS ON EMC and IEEE TRANSACTIONS ON CPMT. He is the Founding Member of the IEEE MTT-RF Nanotechnology Committee.